Composites Part B 226 (2021) 109349

Contents lists available at ScienceDirect

Composites Part B

journal homepage: www.elsevier.com/locate/compositesb

Cold sintered composites consisting of PEEK and metal oxides with improved electrical properties via the hybrid interfaces

Mingming Si [a], Jing Guo [a,*], Jianyu Hao [b], Xuetong Zhao [c], Clive A. Randall [d], Hong Wang [a,b,e]

[a] State Key Laboratory for Mechanical Behavior of Materials & School of Materials Science and Engineering, Xi'an Jiaotong University, Xi'an, 710049, China
[b] School of Electronic and Information Engineering, Xi'an Jiaotong University, Xi'an, 710049, China
[c] State Key Laboratory of Power Transmission Equipment & System Security and New Technology, Chongqing University, Shapingba District, Chongqing, 400044, China
[d] Materials Research Institute and Department of Materials Science & Engineering, The Pennsylvania State University, University Park, PA, 16802, USA
[e] Department of Materials Science and Engineering & Shenzhen Engineering Research Center for Novel Electronic Information Materials and Devices, Southern University of Science and Technology, Shenzhen, 518055, China

ARTICLE INFO

Keywords:
Inorganic-organic composites
Cold sintering process
Zinc oxide
Dielectrics
Varistors

ABSTRACT

The manipulation of interfacial structures offers an effective route to improve the physical and chemical properties of materials. However, it is challenging to design ceramic-based composites with hybrid interfaces involved with organics and inorganics through the conventional sintering technique, due to the incompatibility of these materials at high temperatures. Here, we propose a strategy to integrate poly-ether-ether-ketone together with several metal-oxide additives into zinc oxide (ZnO) to form composite varistors via cold sintering process. Nanoscale layers of hybrid additives are dispersed between densified ZnO grain structures forming Schottky barriers, which dramatically improves the electrical properties of the resulted composites. Compared with pure ZnO, the breakdown electric field at 0.1 mA mm^{-2} reaches over 13 kV mm^{-1}. Particularly, the composite shows a switch-like effect similar with switching devices, with an extraordinarily high nonlinear coefficient of 375. In addition, the elastic module decreases with the addition of PEEK. Given the flexibility in the dopants of polymers and metal oxides, this work provides a unique route to design composite materials with superior performances.

1. Introduction

Varistors are variable resistors with nonlinear electrical (current-voltage) characteristics, which are widely used as surge protection devices and voltage regulators in electrical and electronic circuits. The external lightning or internal switching of the circuit system may lead to transient overvoltage, which results in the abnormal current and damages the components of the system [1,2]. The varistors placed in a suitable position can clamp the voltage and absorb the excess current, thereby protecting sensitive devices. Nonlinear coefficient (α) and breakdown electric field (E_b) are two of the most important parameters for varistor materials [3]. Large α means varistors are sensitive to the overvoltage in the system and high E_b could realize the miniaturization of the devices. In addition, mechanical properties may be also considered in engineering applications.

The chemical properties and physical structures of the interfaces have significant impacts on the performances of both structural and functional materials [4,5], and thus, the tailoring of interfacial structures has attracted much attention in the development of novel materials with unique properties [6,7]. In the case of varistor materials, the interfacial structure is the key factor to generate Schottky effect and result in the nonlinear ohmic characteristics [7–11]. At present, the most commonly used varistor materials are based on ZnO, $SrTiO_3$, $CaCu_3Ti_4O_{12}$ (CCTO), SnO_2 and SiC, etc [1,12–16]. Among all of these materials, ZnO is a typical n-type semiconductor, which has been widely used in commercial varistors. To improve the electrical properties of ZnO varistors, some metal oxides are usually added, such as Bi_2O_3, V_2O_5, Co_2O_3, MnO_2, Cr_2O_3, Sb_2O_3, TiO_2, etc. [17,18]. With different kinds of metal-oxide additives, the nonlinear coefficient and E_b of ZnO varistors can reach 100 and 1000 V mm^{-1}, respectively.

The traditional sintering temperature of ZnO is in the range of 1000–1200 °C, and a lot of researchers have reduced it to 600–1000 °C by hot press, microwave sintering, spark plasma sintering (SPS) et al. in recent years [19]. Cold sintering process (CSP) proposed by the group at

* Corresponding author.
E-mail address: jingguo19@xjtu.edu.cn (J. Guo).

https://doi.org/10.1016/j.compositesb.2021.109349
Received 20 July 2021; Received in revised form 20 September 2021; Accepted 22 September 2021
Available online 24 September 2021

the Pennsylvania State University further lowers the sintering temperature of ZnO to ≤ 300 °C [20,21]. Cold sintering process is a term that covers several different mechanisms and the critical enabling parameter is a transient chemical phase that activates the dissolution and precipitation process, together with a moderate temperature and pressure [22].

The lower sintering temperature enabled by the cold sintering process [23–26], makes it feasible to integrate polymers into grain boundaries of the ceramics [27,28]. Zhao et al. have introduced a ZnO-PTFE (Poly-tetra-fluoroethylene) nanocomposite varistor via the cold sintering process at 285 °C. The E_b of the optimum sample (10 vol% PTFE) is increased to ~3225 V mm^{-1}, with a nonlinear coefficient of 4.23 [29]. Ndayishimiye et al. have fabricated the ZnO-PDMS (Poly--dimethylsiloxane) composites via cold sintering with the in-situ polymerization of a thermoset. The (1−x)ZnO-xPDMS composites (0.00≤ x ≤ 0.05 vol%) cold sintered at 250 °C under a pressure of 320 MPa for 60 min show high relative densities of above 90% [30]. In addition, in our previous work [31], we successfully prepared ZnO/PEEK composites using two different mixing processes together with cold sintering process, and found that the solution method with the aid of tetrahydrofuran and toluene could effectively promote the dispersibility of PEEK in the ZnO matrix. The feasibility of co-firing ceramics with polymers via cold sintering process inspires us to develop high-performance composites with both polymer and metal-oxide additives.

In typical ZnO based varistors, thin layers of metal oxides such as Bi_2O_3, Cr_2O_3, Sb_2O_3, etc. are located at the grain boundaries forming Schottky barriers, which contribute to the nonlinear characteristics of the ceramics [31]. In this work, Poly-ether-ether-ketone (PEEK) and metal oxides including Bi_2O_3, MnO_2, Co_2O_3, Cr_2O_3 are selected to co-fire with ZnO using cold sintering process and to design the interfacial structures of the composites. PEEK is an insulating thermoplastic polymer with a melting point of ~350 °C [32], making it promising to co-fire with ZnO via cold sintering process. It shows excellent temperature and chemical resistance, and can be used as a high temperature resistant structural material and electrical insulation material [33,34]. It is anticipated that unique physical properties, such as low weight, high electrical breakdown strength, and high nonlinear coefficient can be obtained with both PEEK and several metal oxides altering the interfacial structures of the composites.

In this work, the densities, microstructures, mechanical properties, direct current (*DC*) and alternating current (*AC*) electrical properties, and Finite Element Method (FEM) analysis of the composites are discussed in detail. We demonstrate that ZnO-PEEK-(Bi_2O_3–MnO_2–Co_2O_3–Cr_2O_3) composites can be successfully densified using cold sintering process with interesting electrical properties, such as an ultra-high E_b and switch-like effect.

2. Experiments

The ZnO powders was obtained from Forsman Scientific (Beijing) Co., Ltd (99.9%) with a particle size of 270–330 nm. PEEK powders were obtained from Jilin Joinature Polymer Co., Ltd. (99%), with an average particle size of 10 μm. Bi_2O_3 (80 nm), MnO_2 (80 nm), Co_2O_3 (30 nm) and Cr_2O_3 (60 nm) were obtained from Beijing Deke Daojin Science and Technology Co., Ltd and the purities of them are all higher than 99.9%. Acetic acid, toluene and tetrahydrofuran (THF) were obtained from Sinopharm Chemical Reagent Co., Ltd. The concentrations of the solutions are all 99%.

2.1. Preparation of powders

According to the formula in Table 1, the ZnO powder was mixed with several metal oxide additives (Bi_2O_3, MnO_2, Co_2O_3, and Cr_2O_3) and the mixed powder was abbreviated as powder Z. Then, the mixed powder was ball milled in ethanol with zirconium balls using a planetary ball mill tank for 4 h, as shown in Fig. 1. The rotating speed for the ball mill was set to 400 r min^{-1}. Afterwards, the mixture was dried in an oven at 90 °C for 12 h.

Table 1
Composition of powder Z(mol%).

Powder Z	ZnO	Bi_2O_3	MnO_2	Co_2O_3	Cr_2O_3
Z0	100.0	-	-	-	-
Z3	98.2	0.8	0.5	0.5	-
Z6	97.7	0.8	0.5	0.5	0.5

The tetrahydrofuran and toluene solution with a volume ratio of 1.1/1.2 were mixed using the magnetic stirring at 75 °C. The stirring speed was set to 1000 r min^{-1} and the stirring time was 2 h. Afterwards, the PEEK powder was added to the uniformly mixed solution (wherein 0.3 g PEEK powder was added to 100 mL mixed solution). Then, the magnetic stirring was continued at 75 °C for 6 h with a stirring speed of 800 r min^{-1}.

Subsequently, according to the formula of ZnPm shown below, powder Z was added to the mixed solution in which PEEK was dissolved. The n in the powder ZnPm is the serial number of powder Z (n = 0, 3, 6), and m is the mass fraction of PEEK (m = 0.25, 0.5, 1, 3 wt%). For example, Z0P0.25 stands for the composition of Z0 and PEEK with the mass ratio of 99.75/0.25. After mixing, the powders were milled in a planetary ball mill tank for 6 h with a speed of 400 r/min. Then, the mixture was dried at 100 °C for 12 h.

2.2. Cold sintering process

As shown in Fig. 1, 1.0 g ZnPm powder and 0.15 g acetic acid aqueous solution were mixed in an agate mortar. The concentration of the acetic acid aqueous solution was 2 mol L^{-1}. After manual grinding, the wetted powder was put into a die and sintered via cold sintering process at 330 °C with a heating rate of 5 °C min^{-1} under a pressure of 300 MPa. After holding for 2 h, the samples were naturally cooled to room temperature.

2.3. Characterization

Densities of cold sintered samples were measured by Archimedes method. Structures were characterized by X-Ray diffraction with Cu Kα radiation (PANalytical Empyrean). The scanning of 2θ angles ranges from 7° to 70° with a step of 0.026°. The Full-Prof was adopted for the XRD Rietveld refinement processing. The Fourier transform infrared (FT-IR) spectra were measured in the wavenumber range from 400 to 4000 cm^{-1} at every 0.4821 cm^{-1} using a Thermo Scientific Nicolet iS5. Microstructures were observed with field emission FE-SEM (Zeiss Gemini 300) and FE-TEM (JEOL JEM-F200 (HR)). The TEM specimens were prepared using the focused ion beam (FIB, FEI Helios NanoLab 600i). Prior to the FIB process, the surfaces of the samples were polished, and sputtered with Au on one side (Sputter coater, Auto Fine Coater, JFC-1600). The Digital Micrograph software was used to study the TEM results.

The samples were polished by the sandpaper for electrical measurements. Au electrodes were sputtered on both sides of the samples. The temperature dependent Current-Voltage data were collected by a high-voltage & high-temperature test system (PolyK, USA) and the nonlinear coefficients were calculated based on the *E-J* curves.

The impedance spectroscopies from 25 to 260 °C were measured in the frequency range of 100 mHz–8 MHz (Electrochemical workstation, Zennium-Pro 43139, ZAHNER, Germany) and the dielectric properties were obtained using Keysight E4990A in 100 Hz–10 MHz. Ideal *RC* circuit components were utilized to fit the impedance data. The FEM was operated using *COMSOL* with Joule Heating and Heat Transfer in Solid (ht) Modules. The compressive stress–strain curves were tested by Electro-mechanical Universal Testing Machines (CMT4202/ZWICK) with the compression rate of 0.1 mm min^{-1}.

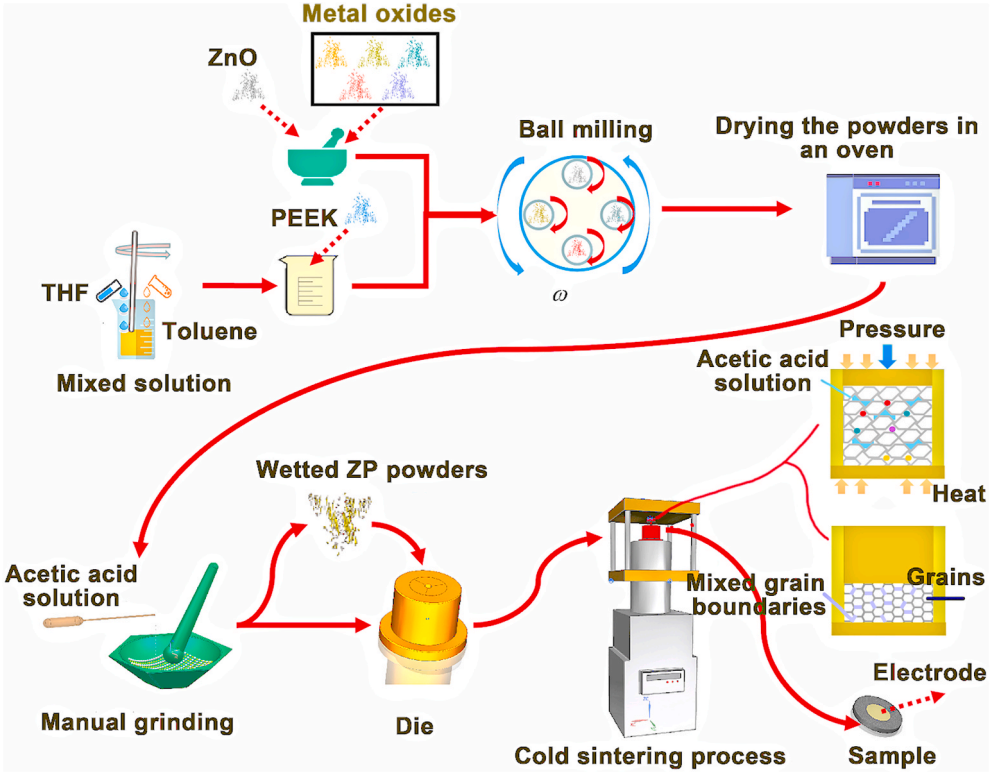

Fig. 1. The schematic of the preparation of ZnO based composites with PEEK and metal oxide additives through the cold sintering process.

3. Results and discussion

3.1. DC electrical performances and switch-like effect

Fig. 2a and Table S1 (Supporting information) show the main performances of typical varistor materials that have been published and commercialized. Fig. 2b presents the *E-J* (electric field-current density) curves of the cold sintered ZnO-PEEK-(Bi_2O_3–MnO_2–Co_2O_3–Cr_2O_3) samples. Fig. 2c and Table S2 (Supporting information) summarize the obtained nonlinear coefficient and E_b at 0.1 mA mm^{-2}. As can be seen, when 0.25 wt% PEEK is added, the E_b of ZnO is significantly improved by ~30 times, indicating that the E_b can be enhanced with the addition of PEEK. PEEK is a good electrical insulation material due to the unique aromatic backbone structure. The breakdown electric field of PEEK is hundreds of times higher that of ZnO, as shown in Table S3 (Supporting information). According to the rules of mixture (ROM) and rule of hybrid mixtures (RoHM) [35–37], the E_b of the composites could be improved with the addition of PEEK. The nonlinear coefficient of ZnO-PEEK composite is only increased slightly compared with pure ZnO, which was also noted earlier with ZnO-PTFE and ZnO-PDMS composites

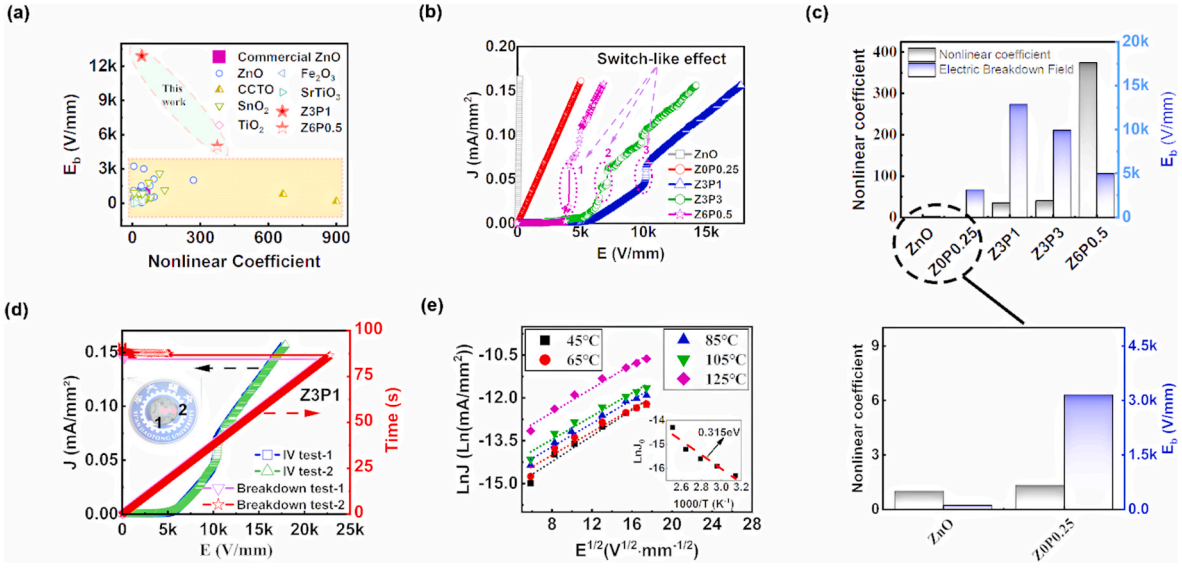

Fig. 2. Comprehensive *DC* electrical properties. a, Performances of varistor ceramics in the references and the cold sintered samples in this work. b, *E-J* curves of pure ZnO, Z0P0.25, Z3P1, Z3P3 and Z6P0.5. c, The nonlinear coefficient and E_b at 0.1 mA mm^{-2} of different samples. d, The comparison between *E-J* curves and electrical breakdown tests (*Time-E* curves) in different areas of the sample Z3P1. e, $E^{1/2}$-*lnJ* curves at 45–125 °C and the calculated activation energy of Z6P0.5.

[29,30].

With more dopants of Bi_2O_3, MnO_2, Co_2O_3, and Cr_2O_3, the nonlinear coefficient can be greatly improved, and the current density shows a dramatic increase in the *E-J* curves (the purple ellipse in Fig. 2b). To our knowledge, this phenomenon is different from the typical *E-J* characteristics of varistors that have been published so far. (Refer to the typical non-ohmic characteristics in Fig. S1, Supporting information). It is similar to the switching effect, although the switching ratio of the composites is lower than that of traditional switching devices. Therefore, we define this interesting effect as the switch-like effect. At the same time, the ZnO based composites with additions of both a hybrid approach with PEEK and Bi_2O_3–MnO_2–Co_2O_3–Cr_2O_3 have ultra-high breakdown electric fields. The maximum E_b at 0.1 mA mm^{-2} reaches almost 13000 V mm^{-1} at room temperature, with a nonlinear coefficient (α) of 41 (sample Z3P1). In addition, the maximum nonlinear coefficient (α) of 375 is obtained in sample Z6P0.5, and its E_b is 5000 V mm^{-1}. The calculated breakdown voltage per grain boundary (V_{gb}) of Z6P0.5 and Z3P1 are 2.89 V gb^{-1} and 9.50 V gb^{-1}, respectively, as shown in Table S4 (Supporting information). Compared with pure ZnO, E_b can be increased by more than 100 times, V_{gb} can be improved by ~40 times, and the nonlinear coefficient α can be increased by over 350 times.

Fig. 2d shows the *E-J* curves and the electrical breakdown strength of different locations in sample Z3P1. The obtained data are similar with each other, revealing that the cold sintered composites have homogeneous microstructures. It also can be seen that the electrical breakdown strength of Z3P1 exceeds 21000 V mm^{-1}, which is much higher than the E_b at 0.1 mA mm^2 (~13000 V mm^{-1}), indicating that the composite varistor can still maintain a safe working state at high current regions.

The comprehensive analysis of Fig. 2b–d demonstrates that PEEK plays a critical role in the E_b and the metal oxides such as Bi_2O_3, MnO_2, Co_2O_3, and Cr_2O_3 have a great influence on the nonlinear coefficient. The varistor effect is mainly due to the doping of Bi_2O_3. In addition, MnO_2, Co_2O_3 and Cr_2O_3 promote the grain boundary resistance of the composite and the barrier height at the grain boundary [18,38]. The details of the effects of Bi_2O_3, MnO_2, Co_2O_3, and Cr_2O_3 on the properties of varistors can be found in the supporting information. ZnO based composites with an ultra-high E_b and excellent nonlinear coefficient can be obtained with the addition of both PEEK and metal-oxide additives through cold sintering process.

Conduction mechanism is the basis for studying the electrical characteristics of varistors and other semiconducting materials. Much effort has been made in the past decades focusing on the conduction mechanism issue in ZnO varistors [16,39–41]. Essentially, it is generally believed that the nonlinear *I–V* characteristic of ZnO varistors is caused by the charge carries transporting across the double-Schottky barrier (DSB) formed at the grain boundaries. As the Fermi level of the n-type semiconducting grain is higher than that of the sandwiched boundary material, electrons flow from the grain to the grain boundary, where they are trapped by the defects and dopants, to increase the local Fermi level until it is the same throughout the structure. At equilibrium, the trapped electrons act as the negative sheet charge at the boundary, leaving behind a layer of positively charged donor sites on either side of the boundary (termed as the depletion layer) that render the energy bands of grains bending upward near the boundary and thus create an electrostatic field with a barrier at the boundary [42–45].

In order to analyze the conduction mechanism of cold sintered ZnO-PEEK-(Bi_2O_3–MnO_2–Co_2O_3–Cr_2O_3) composites, temperature dependent *E-J* characteristics of sample Z6P0.5 have been studied, as shown in Fig. 2e. The Schottky emission current depends on the temperature and electric field that follows Equation (1) [29]:

$$J = AT^2 exp(\beta E^{\frac{1}{2}} - q\varnothing) \quad (1)$$

where J is the current density, A is a constant, T is the absolute temperature, β is a constant, E is the applied electrical field, q is the charge, and $\varnothing$ is the Schottky barrier height. There is a linear relationship between $E^{1/2}$ and lnJ at low electric fields, as shown in Fig. 2e, indicating that Schottky emission current dominates the conduction mechanism of the composites at low electric fields. The calculated activation energy for Schottky emission (Φ) is ~0.32 eV (The details for the calculation can be found in Extended information #1 and Table S5 in Supporting information), which is close to the data of ZnO-PTFE [29].

As shown in Fig. S2 (Supporting information), the *E-J* characteristics of the samples have been tested at different temperatures from −50 to 125 °C. At −50 °C, the nonlinear coefficient of the composite varistor reaches ~600.

3.2. AC electrical performances and finite element analysis

Fig. 3a shows the frequency dependent permittivity of the cold sintered samples at room temperature. It is seen that the permittivity decreases with increasing the frequency in the range of 100 Hz to 10 MHz. Due to the low permittivity of PEEK (ε_r = 3.45–3.50, 1 kHz–10 MHz) [46], the permittivity of ZnO based composites with PEEK and metal-oxide additives is lower than that of pure ZnO ceramics [47]. In the case of the same ratio of added metal-oxides (Z3P1 and Z3P3), the permittivity of the composites decreases with increasing the amount of PEEK. From the frequency dependent dielectric loss as shown in Fig. 3b, a bump is observed in cold sintered ZnO ceramics in the frequency range of 30 kHz–180 kHz, resulting from the electron relaxation process of intrinsic defects [42,48].

Impedance spectroscopy can be used to study the electrical properties of grain boundaries. Therefore, the impedance spectroscopy technique has been adopted to further study the conduction mechanisms of the ZnO-PEEK-(Bi_2O_3–MnO_2–Co_2O_3–Cr_2O_3) composite varistors. Fig. 3c shows a Nyquist plot of the impedance of cold sintered composites at room temperature. The complex impedance (Z) data can be interpreted using *RC* (*R*, resistance; *C*, capacitance) equivalent circuit model, where the ZnO grains are connected in series with grain boundaries composed of PEEK and metal oxides. The grain (R_g) and grain boundary (R_{gb}) resistance can be obtained from the intercept at the high and low frequency limit, respectively. It is seen that R_{gb} is in the range of 10^{10}–10^{11} Ω. As shown in Table S6 (Supporting information), with increasing the amount of PEEK from 1 wt% (Z3P1) to 3 wt% (Z3P3), R_{gb} is increased from 2.294×10^{11} to 3.541×10^{11} Ω, indicating that PEEK has a significant effect on the grain boundary resistance. In addition, the obtained grain resistances of all the samples are around 32–36 Ω, revealing that the PEEK and metal oxide additives of Bi_2O_3–MnO_2–Co_2O_3–Cr_2O_3 have little influence on the grain resistance, as would be expected as the diffusional process in cold sintering is limited to the grain boundary diffusion, and there is no bulk diffusion, or extensive grain growth under the conditions used here.

Fig. 3d shows the temperature dependence of the complex impedance of the sample Z6P0.5. The resistance decreases with increasing temperature and follows the Equation (2) [29]:

$$R = R_0 exp(\frac{E_A}{K_B T}) \quad (2)$$

Where R_0 is a constant, E_A is the activation energy, K_B is the Boltzmann constant, and T is the absolute temperature. The activation energy of the grain boundary resistance is extracted from the Arrhenius plot, as shown in Fig. 3e. The Arrhenius plot shows a feature with two slopes and the calculated activation energy is changed at the temperature of 95–100 °C, which is associated with the defects at the grains and mixed grain boundaries [48]. In the low temperature region, the composite shows a relative low activation energy ranging from 0.35 to 0.39 eV, which may be contributed from the oxygen vacancy. The activation energy at the high temperature region may result from the oxygen chemisorption or interfacial polarization [49–51].

In order to further study the conduction mechanism of the grain boundary, a thermal-electric coupling simulation has been conducted

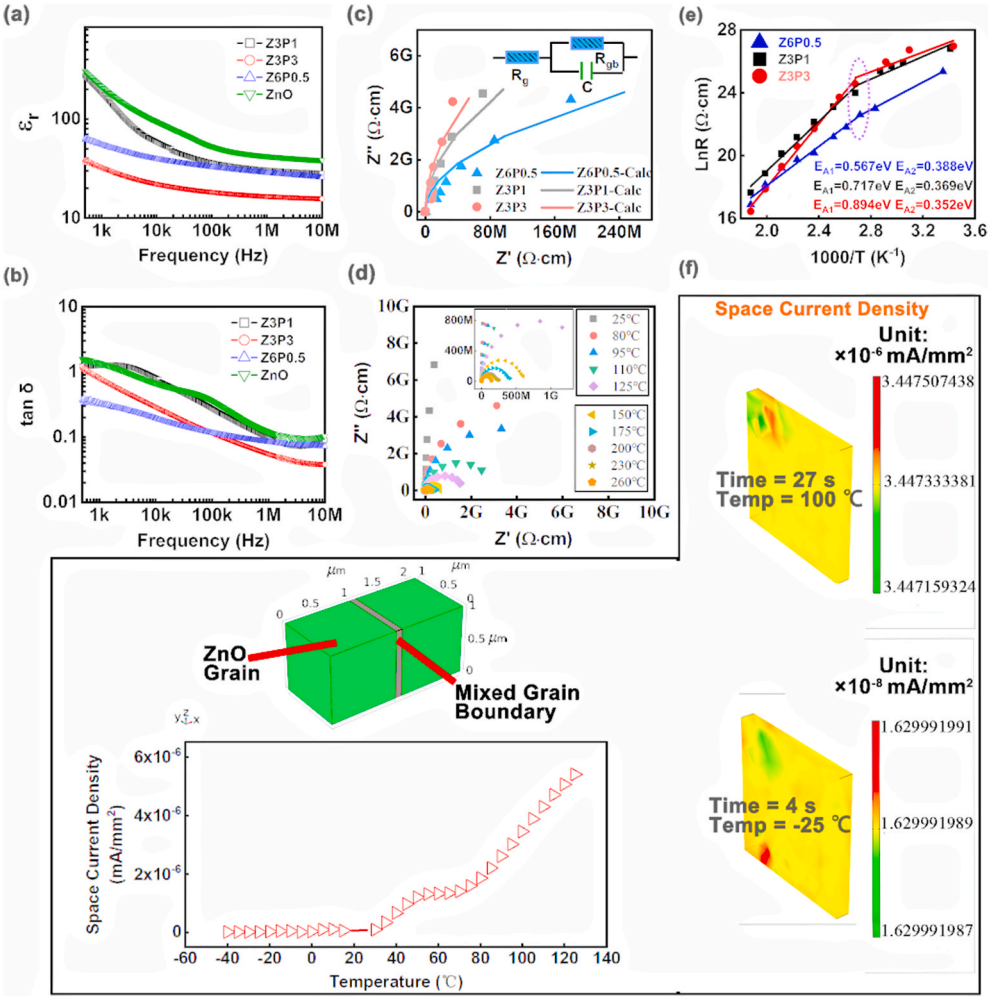

Fig. 3. *AC* electrical properties and FEM analysis. a–b, The permittivity (a) and tan δ (b) in the frequency range of 100 Hz–10 MHz. c, Impedance spectra of cold sintered composites at room temperature. The coefficients of determination for the fitting of impedance data can be found in Table S7 (Supporting information). d, The temperature dependent impedance spectra of sample Z6P0.5. e, The Arrhenius plot and calculated activation energy. The coefficients of determination for the fitting of Arrhenius plot can be found in Table S8 (Supporting information). f, The thermo-electric coupled finite element simulation model, the effective space current density at the grain boundary calculated with FEM and the spatial current density cloud map at −25 and 100 °C.

using finite element method (FEM). To simplify the calculation, the following assumptions are made: two cubes with a side length of 1 μm are established as ZnO grains, and a cuboid with a width of 0.1 μm is established as a mixed grain boundary. The mixed grain boundary is composed of PEEK and metal-oxides. The model is shown in Fig. 3f and the detailed parameters of materials can be found in Fig. S3 (Supporting information). In the thermal-electric coupling calculation, a voltage potential of 0.01 V is applied on the ends of the grains and the temperature range is from −40 to 125 °C.

Fig. 3f and Fig. S4 (Supporting information) show the FEM calculation results. It is observed that as the temperature increases, the maximum value of the current density in the grain boundary shows an increasing trend. It demonstrates that the resistivity of the grain boundary decreases with the temperature increasing, which is in a good agreement with the results of the temperature dependent electrical properties shown in Fig. 3d.

Since the grain boundary is a combination of organic material and metal oxides, the temperature dependent electrical performances can be considered to be anisotropic. Due to the anisotropy, the space current density distribution is not homogeneous in the grain boundary, as shown in Fig. 3f and Fig. S4 (Supporting information), which indicates that the location with a larger current density is more easily to be broken-down. Therefore, it is speculated that there is a connection between the switch-like effect and the compositions and microstructures of the grain boundaries.

3.3. *The microstructures leading to ultra-high breakdown performances and switch-like effect*

According to the combination of electrical performances and FEM results, it is inferred that the high breakdown strength and switch-like effect are closely related to the microstructures, especially the grain boundary features. Therefore, a detailed microstructural analysis has been performed including SEM and TEM.

Relative densities of all the cold sintered samples are shown in Fig. 4a and Fig. S5 (Supporting information). Z3P3 has a relative density of 87%, and all the other samples are densified to over 90%, indicating that cold sintering process is a promising technique to densify ZnO with PEEK and metal oxide additives. Fig. 4b shows the XRD patterns of the samples after cold sintering process. The XRD peaks representing ZnO and Bi_2O_3 can be clearly detected and no impure phases can be observed, revealing that ZnO, PEEK and the metal oxide additives of Bi_2O_3, MnO_2, Co_2O_3, and Cr_2O_3 coexist with cold sintering process. It is also noted that the peaks of other metal oxide additives (Co, Cr, Mn) are not obvious because the content of these additives are small. As a polymer, the XRD peaks of PEEK are broad and weak, and not obvious with the amount in the range of 0–3 wt%. Fig. 4c, Fig. S6 and Table S9 (Supporting information) show the structural refinement results of the pure ZnO, Z0P0.25 and Z6P0.5. The cell parameters of ZnO in Z0P0.25 and Z6P0.5 have little changes compared with those of pure ZnO.

FT-IR has been employed to detect the existence of PEEK. Fig. 4d shows the FT-IR spectra of cold sintered ZnO and ZnO based composites. The aromatic skeleton, ether bond (C–O–C), aromatic hydrogen and the

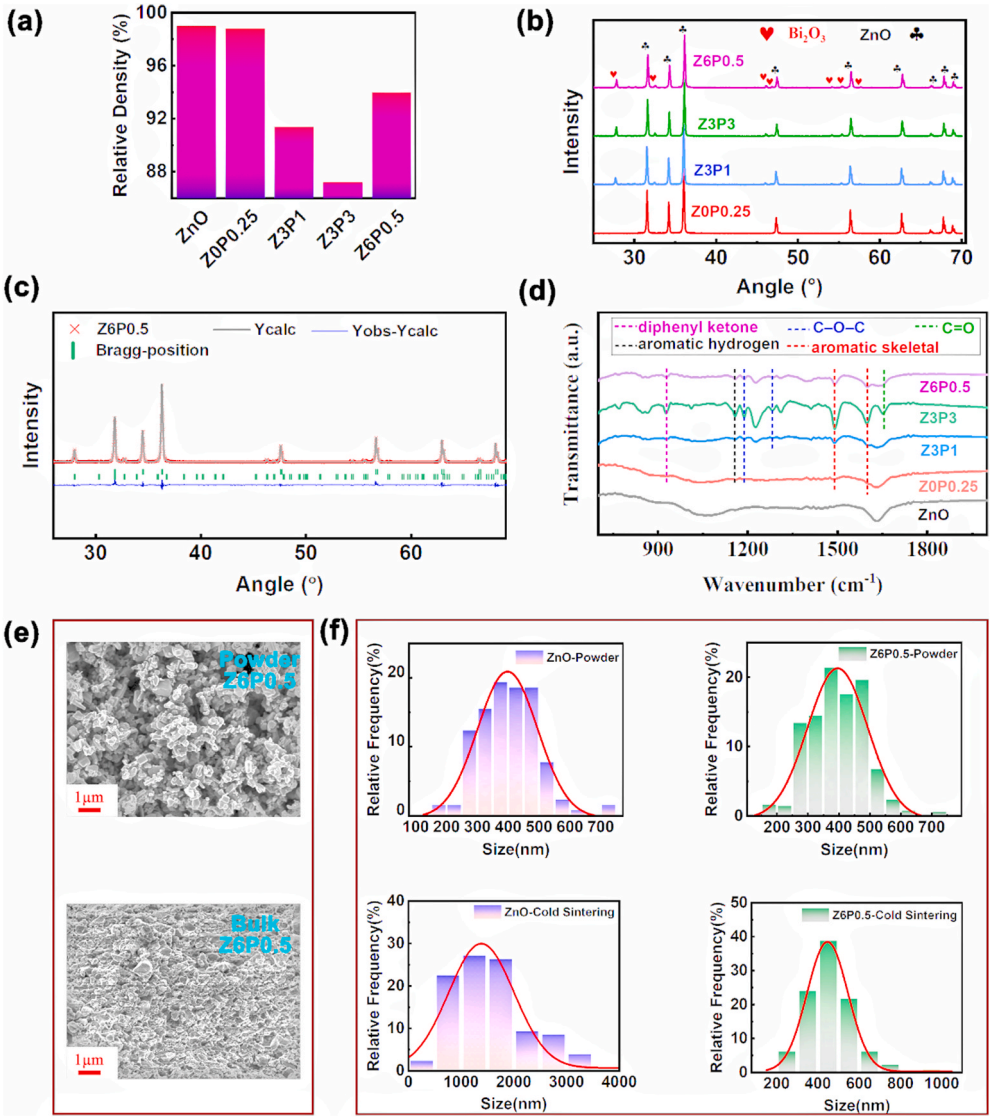

Fig. 4. Densities, structures, and micro-morphologies. a, The relative densities. b, The XRD patterns. c, The structural refinements of Z6P0.5. d, The FT-IR spectra. e, The SEM images of Z6P0.5 raw powder and cross sections of cold sintered Z6P0.5. f, The particle size distribution of ZnO and Z6P0.5 raw powder, and cold sintered ZnO and Z6P0.5.

diphenyl ketone are detectable in all the composite samples, and the ketone group (C═O) is observed in the sample Z3P3 with the highest amount of PEEK (3 wt%). The FT-IR results are consistent with the literatures on the PEEK materials [52,53], demonstrating that PEEK survives under the cold sintering conditions. Fig. 4e present the SEM images of Z6P0.5 powder and cold sintered sample, respectively. After the cold sintering process, the powder is sintered to a dense ceramic, and few pores can be observed. The SEM micrographs of other samples can be found in Fig. S7 (Supporting information).

Fig. 4f shows the particle size distribution of raw powders and cold sintered samples of ZnO and Z6P0.5. It can be clearly seen that the ZnO grains grow from 330 nm to 2–3 μm in the pure ZnO samples prepared by cold sintering process at 330 °C for 2 h under a pressure of 300 MPa. For the composites with PEEK and various metal oxide additives under the same cold sintering condition, there is only slight change in the particle size of ZnO, indicating that the PEEK and metal oxide additives located at the grain boundaries effectively suppress the grain growth of ZnO during the cold sintering process. The areas of grain boundaries increase with smaller grain size, which is beneficial to the improvement of the breakdown electric field, nonlinear coefficient and grain boundary resistance [54].

The interfacial structures of the ZnO-PEEK-(Bi_2O_3–MnO_2–Co_2O_3–Cr_2O_3) composites are further studied using high resolution TEM, as shown in Fig. 5 and Fig. S8 (Supporting information). PEEK is dissolved in a mixed solution of tetrahydrofuran and toluene, and cold co-sintered with ZnO together with metal-oxide additives. Element C, Bi, Mn, Co, and Cr are observed along the grain boundary, as shown in Fig. 5a, indicating that the PEEK and metal-oxide additives are dispersed in ZnO matrix forming complex grain boundaries after cold sintering process. It can be seen in Fig. 5b that the main component of the grain boundaries is Bi_2O_3. In addition, some metal-oxide nanocrystals and polymers in the range of several nanometers could be observed in the grain boundary. The EDS mapping results in Fig. S8 (Supporting information) further indicate that the hybrid grain boundaries are constituted by PEEK and metal oxides.

Fig. 5c–h show the thin grain boundaries with several nanometers, including hybrid interfaces (Fig. 5c–d), ZnO-PEEK interfaces (Fig. 5e–f) and ZnO–ZnO interfaces (Fig. 5g–h). The polymer phase is identified by the Fast Fourier Transform (FFT) calculation as shown in Fig. 5e–f. The crosslink sites of PEEK in the grain boundaries may offer traps for the charges, which can improve the electrical properties of composites [55]. It is pointed out that the overall performances of varistors are generally

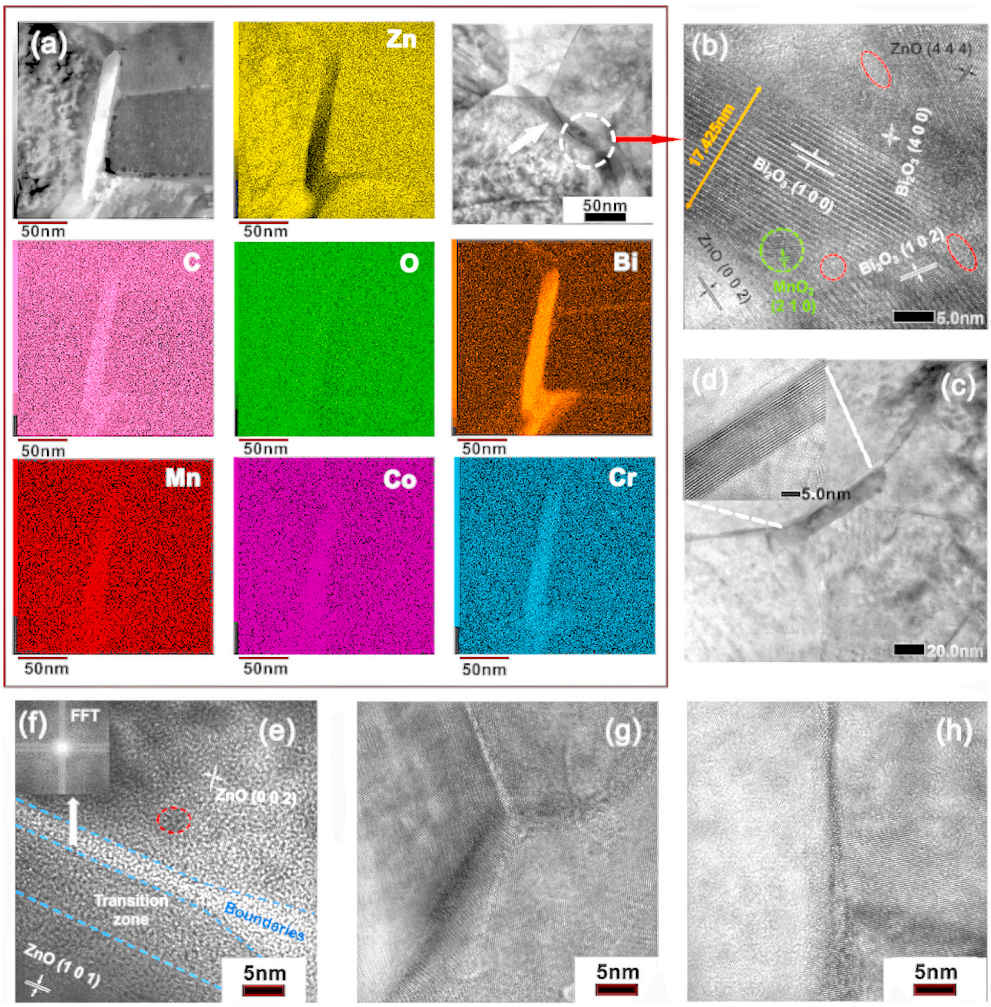

Fig. 5. High resolution TEM and EDS mapping of cold sintered Z6P0.5. a, The TEM and corresponding EDS results of the hybrid grain boundary. b–d, HRTEM micrographs corresponding to Fig. 5a. f–h, HRTEM micrographs showing the typical grain boundaries.

enhanced with thinner grain boundaries [56]. Therefore, it is inferred that the structures of the complex grain boundaries of the composites dominate the unique electrical performances, such as the ultra-high E_b and switch-like effect.

Fig. S9 (Supporting information) depicts the mechanical properties of the samples prepared by cold sintering process. It is seen that the elastic module decreases from 1222 MPa (pure ZnO) to 711 MPa (Z3P3) with increasing the amount of PEEK. It is demonstrated that the flexibility of the composites can be improved with the addtion of PEEK.

4. Conclusions

The strategy of hybrid interface design has been adopted via cold sintering process in this work. The highly insulating thermoplastic polymer (PEEK) has been dissolved through a mixed solution of tetrahydrofuran and toluene. The dissolved PEEK, metal oxides (Bi_2O_3–MnO_2–Co_2O_3–Cr_2O_3) and ZnO matrix were densified by cold sintering process at 330 °C and 300 MPa for 2 h forming inorganic-organic composites. Thin layers of hybrid grain boundaries including metal oxides and polymers were observed using HRTEM, and some nanocrystals and polymers in the range of several nanometers were detected in the grain boundaries. The unique interfacial structures significantly improve the electrical properties of ZnO-based composites, such as E_b and nonlinear coefficients. Particularly, a unique phenomenon — switch-like effect can be observed. The E_b of the composite varistor reaches up to 13 kV mm^{-1}, and the maximum nonlinear coefficient exceeds over 300. The temperature dependent *E-J* characteristics indicate that Schottky emission current dominates the conduction mechanism of the composites at low electric fields, and the calculated activation energy for Schottky emission is ~0.32 eV. The impedance data reveal that the PEEK and metal oxide additives have a significant effect on the grain boundary resistance. The temperature dependence of the complex impedance shows a feature with two slopes and the calculated activation energy is changed at the temperature of 95–100 °C, which is associated with the defects at the grains and mixed grain boundaries. The FEM analysis further demonstrates that the resistivity of the grain boundary decreases with the temperature increasing and the space current density distribution is not homogeneous in the grain boundary. At the same time, the flexibility of the composites has been improved by the addition of PEEK. In summary, the concept of integrating multiple organic and inorganic materials and altering the interfacial structures using the dissolution mixing method together with cold sintering process offers a promising route to develop new generation composites with improved functionalities.

Author contributions

J.G. and M.S. conceived the idea. J.G. and H.W. supervised the entire project. M.S. prepared the samples and performed the electrical characterizations with the help of J.H. and X.Z. M.S. conducted the FEM simulations and analyzed the data with the help of J.G. and C.A.R. J.G. and M.S. wrote the manuscript. All the authors discussed and

contributed to the manuscript revision.

Declaration of competing interest

The authors declare that they have no known competing financial interests or personal relationships that could have appeared to influence the work reported in this paper.

Acknowledgements

This work was supported by the National Natural Science Foundation of China (51902245, 51877016) and Natural Science Foundation of Shaanxi Province (2020JQ-044). We thank Zijun Ren, Yanan Chen, Jiao Li, Yang Zhang and Chao Li (The Instrument Analysis Center of Xi'an Jiaotong University) for the SEM and FE-TEM measurements. We thank Lu Lu and Hu Nan (The School of Microelectronics and State Key Laboratory for Mechanical Behaviour of Materials, Xi'an Jiaotong University) for preparing the specimens via FIB and FE-TEM measurements.

Appendix A. Supplementary data

Supplementary data to this article can be found online at https://doi.org/10.1016/j.compositesb.2021.109349.

References

[1] Tian T, Zheng L, Podlogar M, Zeng H, Bernik S, Xu K, Ruan X, Shi X, Li G. Novel ultrahigh-performance ZnO-based varistor ceramics. ACS Appl Mater Interfaces 2021;13:35924–9.
[2] Manjula NM, Chen SM. One-pot synthesis of rod-shaped gadolinia doped zinc oxide decorated on graphene oxide composite as an efficient electrode material for isoprenaline sensor. Compos B Eng 2021;211:108631.
[3] Kazuo E. Conduction mechanism of nonohmic zinc oxide ceramics. J Appl Phys 1978;49:2964–72.
[4] Cruickshank AC, Tay SER, Illy BN, Campo RD, Schumann S, Jhones TS, Heutz S, Mclachlan MA, Macomb DW, Riely DJ, Ryan MP. Electrodeposition of ZnO nanostructures on molecular thin films. Chem Mater 2021;23:3863–70.
[5] Pan T, Jiang JH, Li JJ, Liu T, Yu S, Sun XT, Yan ZC, Chen SJ, Fan Y, Gao M, Deng X, Liu TJ, Yao DZ, Xia Y, Lin Y. The ferroelectric ceramic/elastomer composite as the dielectric coating of soft capacitive neural interface: the competitive effects of ceramic particles. Compos B Eng 2021;204:108475.
[6] Chen JZ, Park NG. Materials and methods for interface engineering toward stable and efficient perovskite solar cells. ACS Energy Lett 2020;5:2742–86.
[7] Simon P, Gogotsi Y. Perspectives for electrochemical capacitors and related devices. Nat Mater 2020;19:1151–63.
[8] Hong YY, Wang Z, Chen LY, Shu SL, Qiu F, Zhang LC, Mccormack DE. Interface formation and bonding control in high-volume-fraction (TiC+TiB_2)/Al composites and their roles in enhancing properties. Compos B Eng 2021;209:108605.
[9] Nadine R, Peter S, Robert D, Michael H. Piezotronically modified double Schottky barriers in ZnO varistors. Adv Mater 1995;6:993–6.
[10] Satoru, Fujitsu, Hiroshi, Toyoda, Hiroaki, Yanagida. Origin of ZnO varistor. J Am Ceram Soc 1987;70:71–2.
[11] Shanenkova YL, Tsimmerman AI, Osokina LV. Creating a composite material ZnO-Bi_2O_3 with a core-shell structure for varistor ceramics. J. Phys.: Conf. Ser. 2019;1347:012040.
[12] Masteghin MG, Varela M, Orlandi MO. Controlling the breakdown electric field in SnO_2 based varistors by the insertion of SnO_2 nanobelts. J Eur Ceram Soc 2017;37:1535–40.
[13] Aljaafari A, Sedky A. Influence of fine crystal percentage on the electrical properties of ZnO ceramic-based varistors. Crystals 2020;10:681.
[14] Tang Z, Wu KN, Li JY, Huang SD. Optimized dual-function varistor-capacitor ceramics of core-shell structured x$Bi_{2/3}Cu_3Ti_4O_{12}$/(1-x)$CaCu_3Ti_4O_{12}$ composites. J Eur Ceram Soc 2020;40:3437–44.
[15] Staykov A, Tellez H, Druce J, Wu J, Ishihara T, Kilner J. Electronic properties and surface reactivity of SrO-terminated $SrTiO_3$ and SrO-terminated iron-doped $SrTiO_3$. Sci Technol Adv Mater 2017;19:221–30.
[16] Kashyap SK, Mitra R. Densification behavior involving creep during spark plasma sintering of ZrB_2-SiC based ultra-high temperature ceramic composites. Ceram Int 2020;46:5028–36.
[17] Bueno PR, Leite ER, Oliveira MM, Orlandi MO, Longo E. Role of oxygen at the grain boundary of metal oxide varistors: a potential barrier formation mechanism. Appl Phys Lett 2001;79:48–50.
[18] He J. Metal oxide varistors: from microstructure to macro-characteristics. Tsinghua University, Press; 2019, ISBN 978-3-527-33382-0.
[19] Wei G, Shu X, Zhang Z, Li Q, Lu X. B_2O_3-Bi_2O_3-ZnO based materials for low-sintering temperature immobilization of iodine adsorbed waste. J Solid State Chem 2020;289:121518.
[20] Guo J, Guo HZ, Amanda LB, Michael TL, Elizabethm RK, Gary ML, Randall CA. Cold sintering: a paradigm shift for processing and integration of ceramics. Angew Chem Int Ed 2016;55:11457–61.
[21] Funahashi S, Guo J, Guo HZ, Wang K, Amanda LB, Kosuke S, Randall CA. Demonstration of the cold sintering process study for the densification and grain growth of ZnO ceramics. J Am Ceram Soc 2017;100:546–53.
[22] Guo J, Floyd R, Lowum S, Maria JP, Beauvoir THD, Seo JH, Randall CA. Cold sintering: progress, challenges and future opportunities. Annu Rev Mater Res 2019;49:275–95.
[23] Nie J, Hu C, Yan Q, Luo J. Discovery of electrochemically induced grain boundary transitions. Nat Commun 2021;12:2374.
[24] Gonzalez J, Neuhaus K, Bernemann M, Peteira DSJ, Laptev A, Bram M, Guillon O. Unveiling the mechanisms of cold sintering of ZnO at 250 degrees C by varying applied stress and characterizing grain boundaries by kelvin probe force microscopy. Acta Mater 2018;144:116–28.
[25] Faouri SS, Mostaed A, Dean JS, Wang D, Sinclair Derek C, Zhang SY, Whittow WG, Vardaxoglou Yiannis, Reaney IM. High quality factor cold sintered Li_2MoO_4-$BaFe_{12}O_{19}$ composites for microwave applications. Acta Mater 2019;166:202–7.
[26] Nie J, Zhang Y, Chan JM, Huang R, Luo J. Water-assisted flash sintering: flashing ZnO at room temperature to achieve ~ 98% density in seconds. Scripta Mater 2018;142:79–82.
[27] Guo J, Berbano SS, Guo H, Baker AL, Lanaga MT, Randall CA. Cold sintering process of composites: bridging the processing temperature gap of ceramic and polymer materials. Adv Funct Mater 2016;26:7115–21.
[28] Guo J, Zhao X, Beauvoir THD, Berbano SS, Seo JH, Baker AL, Azina C, Randall CA. Recent progress in the cold sintering process of ceramic-polymer composites. Adv Funct Mater 2018;28:1801724.
[29] Zhao X, Guo J, Wang K, Thomas H, Li B, Randall CA. Introducing a ZnO-PTFE (polymer) nanocomposite varistor via the cold sintering process. Adv Eng Mater 2018;20:1700902.
[30] Ndayishimiye A, Grady ZA, Tsuji K, Wang K, Bang SH, Randall CA. Thermosetting polymers in cold sintering: the fabrication of ZnO polydimethylsiloxane composites. J Am Ceram Soc 2020;103:3039–50.
[31] Si MM, Hao JY, Zhao ED, Zhao XT, Guo J, Wang H, Randall CA. Preparation of zinc oxide/poly-ether-ether-ketone (PEEK) composites via the cold sintering process. Acta Mater 2021;215:177036.
[32] Gas Gupta DK, Doughty K. Dielectric and conduction processes in polyetherether ketone (PEEK). IEEE Trans Electr Insul 1987;22:1–7.
[33] Dumonceaux TJ, Hill JE, Pelletier CP, Paice MG, Van Kessel AG, Hemmingsen SM. The effect of insulating layers on the performance of implanted antennas. IEEE Trans Antenn Propag 2011;59:21–31.
[34] Lafi AGA, Alzier A, Allaf AW. Two-dimensional FTIR spectroscopic analysis of crystallization in cross-linked poly(ether ether ketone). International Journal of Plastics Technology 2020;24:1–8.
[35] Tan LJ, Zhu W, Zhou K. Recent progress on polymer materials for additive manufacturing. Adv Funct Mater 2020;30:2003062.
[36] Mansor MR, Sapuan SM, Zainudin ES, Nuraini AA. Stiffness prediction of hybrid kenaf/glass fiber reinforced polypropylene composites using rule of mixtures (ROM) and rule of hybrid mixtures (RoHM). J Polym Mater 2013;30:321–34.
[37] Yuan S, Shen F, Chua CK, Zhou K. Polymeric composites for powder-based additive manufacturing: materials and applications. Prog Polym Sci 2019;91:141–68.
[38] Carlsson JM, Domingos HS, Bristowe PD, Hellsing B. An interfacial complex in ZnO and its influence on charge transport. Phys Rev Lett 2003;16:165506.
[39] Chung SY, Kim ID, Kang SJL. Strong nonlinear current-voltage Behaviour in perovskite-derivative calcium copper titanate. Nat Mater 2004;3:774–8.
[40] Blatter G, Greuter F. Electrical breakdown at semiconductor grain boundaries. Phys Rev B Condens Matter 1986;34:8555–72.
[41] Levinson LM, Philipp HR. The physics of metal oxide varistors. J Appl Phys 1975;46:1332–41.
[42] Mahan GD, Levinson LM, Philipp HR. Theory of conduction in ZnO varistors. J Appl Phys 1979;50:2799–812.
[43] Pike GE. Semiconductor grain-boundary admittance: theory. Phys Rev B Condens Matter 1984;30:795–802.
[44] Sato Y, Buban JP, Mizoguchi T, Shibata N, Yodogawa M, Yamamoto T, Ikuhara Y. Role of Pr segregation in acceptor-state formation at ZnO grain boundaries. Phys Rev Lett 2006;97:106802.
[45] Tsuj K, Chen WT, Gu H, Lee WH, Fritsch SG, Randall CA. Contrasting conduction mechanisms of two internal barrier layer capacitors: (Mn, Nb)-doped $SrTiO_3$ and $CaCu_3Ti_4O_{12}$. J Appl Phys 2017;121:064107.
[46] Sun H, Lv Y, Zhang C, Zuo X, Li M, Yue X, et al. Materials with low dielectric constant and loss and good thermal properties prepared by introducing perfluorononenyl pendant groups onto poly(ether ether ketone). RSC Adv. 2018;8:7753–60.
[47] Guo J, Zhou D, Li Y, Shao T, Wang H. Structure-property relationships of novel microwave dielectric ceramics with low sintering temperatures: ($Na_{0.5x}Bi_{0.5x}Ca_{1-x}$)$MoO_4$. Dalton Trans 2014;43:11888–96.
[48] Hunter CC, Sinclair DC, West AR, Hooper A. AC impedance studies of the lithium/polymer electrolyte interface in solid-state lithium cells. J Power Sources 1988;24:157–64.
[49] Chiou BS, Chung MC. Admittance spectroscopy and trapping phenomena of ZnO based varistors. J Electron Mater 1991;20:885–90.
[50] Lagowski J, Sproles ES, Gatos HC. Quantitative study of the charge transfer in chemisorption; oxygen chemisorption on ZnO. J Appl Phys 1977;48:3566–75.
[51] Mitra P, Chatterjee AP, Maiti HS. ZnO thin film sensor. Mater Lett 1998;35:33–8.

[52] Ding SY, Yi J, Li JF, Ren B, Tian ZQ. Nanostructure-based plasmon-enhanced Raman spectroscopy for surface analysis of materials. Nat. Rev. Mater. 2016;1:16021.
[53] Li H, Yang J, Tian F, Li X, Dong S. Study on the microstructure of polyether-ether-ketone films irradiated with 170 keV protons by grazing incidence small angle X-ray scattering (GISAXS) Technology. Polymers 2020;12:2717.
[54] Sun HT, Zhang LY, Yao X. Electrical nonuniformity of grain boundaries within ZnO varistors. J Am Ceram Soc 1993;76:1150–5.
[55] Giants TW. Crystallinity and dielectric properties of PEEK, poly(ether ether ketone). IEEE Trans Dielectr Electr Insul 1994;1:991–9.
[56] Zhao X, Liang J, Sun J, Guo J, Randall CA. Cold sintering ZnO based varistor ceramics with controlled grain growth to realize superior breakdown electric field. J Eur Ceram Soc 2021;41:430–5.